Multiband stereometamaterial-based polarization spectral filter

J. H. Shi,[1,2,*] H. F. Ma,[2] W. X. Jiang,[2] and T. J. Cui[2,†]

[1]*College of Science, Harbin Engineering University, Harbin 150001, China*
[2]*State Key Laboratory of Millimeter Waves, Southeast University, Nanjing 210096, China*

We propose a kind of stereometamaterial composed of periodic structures with twisted asymmetrical split-ring (ASR) resonators. The proposed stereometamaterial has intrinsic chirality and can be used as a multiband polarization spectral filter. Full-wave simulation and experimental results demonstrate that the stereometamaterial with the twist angle of $\phi = 90°$ exhibits three ripple-free cross-polarization transmission peaks at normal incidence of plane waves. The cross-polarization transmission bands are centered at the maxima of circular dichroism, accompanied by pairs of pure circular birefringence points. In physics, the near-field electric and magnetic coupling of orthogonal ASR molecules in parallel planes contributes to the conversion of two orthogonal linear polarizations. The transmission of the proposed multiband polarization spectral filter can be engineered via the mutual twist angle and asymmetry of the ASRs and the thickness of the dielectric spacer layer and also be tuned via the angle of incidence.

During the past decade, metamaterials consisting of artificial "atoms" or "molecules" that are engineered to have properties unavailable in nature (e.g., negative refraction) have attracted a tremendous amount of interest.[1–3] Metamaterials offer a versatile way to manipulate propagation of electromagnetic (EM) waves, particularly to tailor the polarization state of light,[4] which is a fundamental characteristic of transverse EM waves. A number of metamaterial-based polarization devices, including the polarization selector,[5] linear and circular polarizers,[6–8] wave retarder,[9] polarization rotator,[10] and polarization filter,[11] have been reported. Metamaterials were also applied to achieve unusual polarization functionalities like asymmetric transmission,[12] negative refractive index,[13–15] and giant optical activity.[16–18] More recently, motivated by the traditional polarization spectral filter suggested by Henry,[19] a narrow-band metamaterial spectral filter with a ripple-free isolated transmission peak has been demonstrated,[20] which is achieved through the exploitation of circular birefringence of a single-layer metamaterial at oblique incidence. The traditional polarization spectral filter mainly depends on the dispersion of linear birefringence around an isoindex point, where linear birefringence vanishes. Although isoindex filters have been extensively studied, the practical applications are extremely hampered by isoindex crystals because there are only a few isoindex crystals available in nature, and they are often extremely expensive. Metamaterial-based polarization spectral filters can be realized for any wavelength from the microwave to the optical domain. The filter allows a narrow transmission band when the metamaterial is placed between two orthogonal linear polarizers.

In the work, we report a multiband polarization spectral filter based on a stereometamaterial consisting of an array of stereo asymmetrical split-ring (ASR) dimers spatially separated by a dielectric layer. Here, each unit cell, or metamolecule, consists of two stacked ASR resonators with identical geometry, which are rotated relative to each other.[21,22] The near-field magnetic and electric coupling of stereo ASR dimers gives birth to linear polarization conversion. Once stereo ASR dimers are orthogonally arranged, the stereometamaterial exhibits three narrow-band ripple-free transmission peaks at normal incidence when it is sandwiched between two orthogonal linear polarizers.

The filter configuration is sketched in Fig. 1(a), which is realized by crossed linear polarizers on either side of the stereometamaterial consisting of asymmetrical molecules (ASRs) on both sides of a dielectric layer. The stereometamaterial has an obvious advantage by reducing the filter dimension along the propagation direction of EM waves compared to the single-layer metamaterial isoindex filter in Ref. 20, where an oblique incidence is necessary to achieve extrinsic chirality,[23] as shown in Fig. 1(b). Furthermore, the proposed bilayered metamaterial patterned on printed circuit board (PCB) has a simple design, which is ideally suited for the existing manufacturing technologies of planar microstructures and nanostructures.

The response of a metamaterial is not simply determined by the behavior of the individual unit cell but is also directly linked to the spatial arrangement of metamolecules involved in an ensemble. Metallic split-ring metamolecules are important building blocks of metamaterial structures. Here, we propose a bilayered stereometamaterial with stereo ASR dimers as a polarization spectral filter. When two stacked ASRs are close to each other, it is predicted that the near-field coupling between two twisted ASRs will affect the far-field polarization state and lead to the polarization rotation and cross-polarization transmission due to the chiral symmetry associated with twist angles other than $\phi = 0°$ and $\phi = 180°$. The stereometamaterials consist of square metamolecule arrays with a period of $d = 15$ mm, rendering the structures nondiffractive at normal incidence for frequencies below 20 GHz. The metamaterial patterns with an overall size of 300×300 mm^2 are etched from 35-μm copper cladding on a FR4 PCB substrate with a thickness of $t = 1.6$ mm. Each stereo ASR dimer consists of two spatially separated ASRs, which are structurally identical but twisted by an angle ϕ. Each ASR consists of two different wire arcs corresponding to open angles $\alpha = 160°$ and $\beta = 140°$, as shown in Fig. 1(c). The ASR radius is $r = 6$ mm, and the metallic line width is $w = 0.8$ mm. The detailed design of the ASR dimer and a photograph of a sample are given in
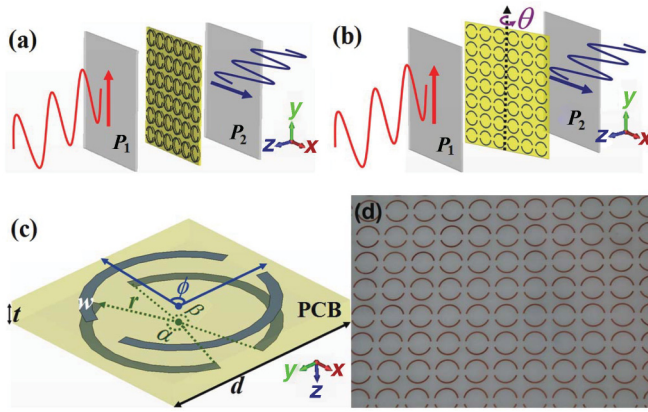
FIG. 1. (Color online) Stereometamaterial spectral filters. (a) The stereometamaterial sandwiched between two orthogonal linear polarizers P_1 and P_2 acts as a cross-polarization spectral filter at normal incidence. The incident wave propagates along the $-z$ direction. The bold arrows denote the polarization directions. (b) The single-layer metamaterial only exhibits strong resonant optical activity at oblique incidence that is realized by tilting the metamaterial around its symmetry axis, which coincides with a zero-birefringence isoindex point. (c) The schematic of a unit cell of the stereo ASR dimer array. The two ASRs are rotated with respect to each other by the twist angle ϕ. Each ASR resonator has two different metallic arcs corresponding to angles α and β. Their central points always lie on the z axis, and one ASR has its symmetry axis along the y direction in all experiments. (d) The top view of a fabricated stereometamaterial sample, which is manufactured from FR4 PCB laminates using the photolithography technique.

Figs. 1(c) and 1(d), respectively. Four samples were fabricated corresponding to twist angles of $\phi = 0°$, $\phi = 45°$, $\phi = 90°$, and $\phi = 180°$.

The stereometamaterial transmission spectra are measured at normal incidence in the frequency range from 4 to 12 GHz. The experiments are carried out in an anechoic chamber using broadband horn antennas and a vector network analyzer. The transmission spectra and the associated modes of excitation are simulated using the commercial software, CST Microwave Studio,[24] in the frequency domain, where copper is treated as a perfect electric conductor and a permittivity $\varepsilon = 4.05 + i \cdot 0.05$ is assumed for the lossy dielectric substrate. In the simulations, the frequency domain solver is used with periodic boundary conditions. Figures 2(a) and 2(b) show the measured and simulated transmission of the stereometamaterial with the twist angle $\phi = 90°$. The transmission coefficient T_{xx} of x-polarized wave coincides with the transmission coefficient T_{yy} of y-polarized wave, because two orthogonal ASRs ensure that the structure is isotropic for observations at normal incidence. As a consequence, there are no linear birefringence and dichroism in the whole frequency range we considered.

The single-layered ASR metamaterial lacking twofold rotational symmetry has been reported to support the so-called trapped mode that is formed by an antisymmetrical current excitation at normal incidence.[25,26] Due to the intrinsic nonchirality, the single-layered ASR metamaterial cannot exhibit optical activity and associated cross-polarization transmission at normal incidence. Fortunately, the stereometamaterial with two orthogonal ASRs reveals three-band cross-polarization
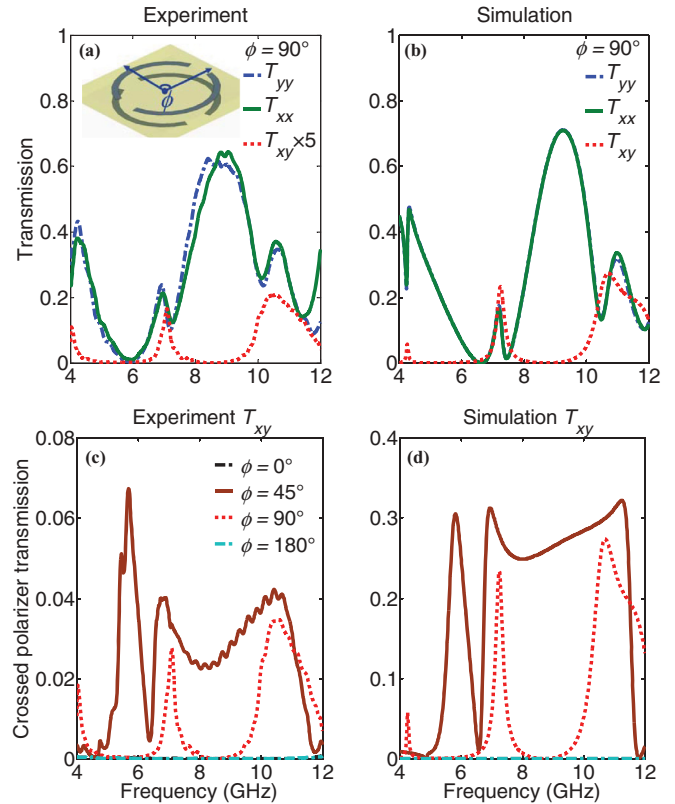

FIG. 2. (Color online) The transmission spectra of stereometamaterial-based polarization spectral filters. (a) Measured and (b) simulated transmission spectra of the stereometamaterial with twist angle $\phi = 90°$. For clarity, the amplitude of the measured cross-polarization transmission is multiplied by a factor of 5. The inset shows a stereo ASR dimer. (c) Measured and (d) simulated cross-polarization transmission spectra of the stereometamaterials with twist angles $\phi = 0°$, $\phi = 45°$, $\phi = 90°$, and $\phi = 180°$ for the y-polarized incident EM waves.

transmission at ∼4, 7, and 11 GHz due to the resonance hybridization resulting from the near-field coupling.[27,28] The measured results agree very well with simulations for the copolarization transmission coefficients (T_{xx} and T_{yy}), compare Figs. 2(a) and 2(b). Here, we remark that the amplitude of the measured cross-polarization transmission has been multiplied by a factor of 5 to make its spectral behavior, which is in good agreement with the simulation results, more visible. The difference in amplitude is most likely caused by underestimating the imaginary part of the permittivity of the FR4 PCB substrate in simulations. Fabrication errors and random errors in experiments may also contribute to the lower cross-polarization transmission in experiments. In order to characterize the dependence of cross-polarization transmission on twist angles, we measured and simulated three other stereometamaterials with twist angles $\phi = 0°$, $\phi = 45°$, and $\phi = 180°$ for the y-polarized incident waves, as demonstrated in Figs. 2(c) and 2(d). For the cases of $\phi = 0°$ and $\phi = 180°$, the stereometamaterials do not show any cross-polarization transmission since the incident polarization state is parallel to a line of mirror symmetry of the structure. In the case of $\phi = 45°$, we notice that the two higher-frequency cross-polarization transmission peaks of the stereometamaterial
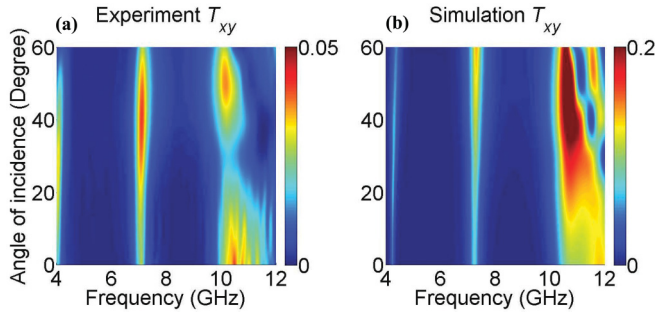
FIG. 3. (Color online) Angular dependence of the stereometamaterial cross-polarization transmission when the twist angle is fixed as $\phi = 90°$.

move towards lower frequencies than those of $\phi = 90°$, while the low-frequency transmission peak vanishes; this is more clearly seen in Fig. 4(a). The associated dramatic change is that the passband at $\sim$11 GHz evolves into a broadband transmission window from 7 to 11 GHz.

The single-layer metamaterial isoindex filter in Ref. 20 is based on extrinsic chirality[23] achieved by an oblique incidence. The performance of the filter is directly modulated via the angle of incidence. Here, we also consider how incidence angles affect the cross-polarization transmission of the stereometamaterial. Figure 3 shows the measured and simulated cross-polarization transmission spectra of the stereometamaterial as a function of incidence angles when the twist angle is fixed as $\phi = 90°$. In the range from $0°$ to $60°$, the spectral positions of the passbands at $\sim$4 and 7 GHz remain unchanged, while the passband at $\sim$11 GHz shifts to lower frequency. The transmission increases when the incidence angle becomes large. Although a relatively large random error happens at $\sim$11 GHz, the measured and simulated results are in good overall agreement.

The dependence of the filter transmission spectra on the twist angle, the dielectric-layer thickness, and the arc angle are investigated individually. In Fig. 4(a), the $90°$-twisted stereometamaterial obviously shows triple-band cross-polarization transmission, while all cross-polarization transmission bands disappear for twist angles of $0°$ and $180°$. The stereometamaterials with intermediate twist angles reveal broadband cross-polarization transmission of up to 50%. When other parameters are kept the same, Fig. 4(b) illustrates the cross-polarization transmission engineered via the dielectric-layer thickness. The transmission bands at 4 and 7 GHz frequencies shift progressively to blue and red with the increasing thickness, respectively. However, the passband at high frequency remains basically fixed at $\sim$11 GHz, and the associated transmission seems to have a peak for an optimal thickness of 1 mm. Interestingly, the transmission amplitude (about 30%) and spectral width of the intermediate passband depend only weakly on the substrate thickness, while its spectral position can be shifted anywhere from 7 to 10 GHz.

Figure 4(c) shows the dependence of the cross-polarization transmission on the ASR asymmetry via changing the arc angle β, provided that other parameters are kept unchanged. When two arc angles α and β are equal to $160°$, the stereometamaterial exhibits no cross-polarization transmission due to twofold rotational symmetry of the split-ring metamolecule.
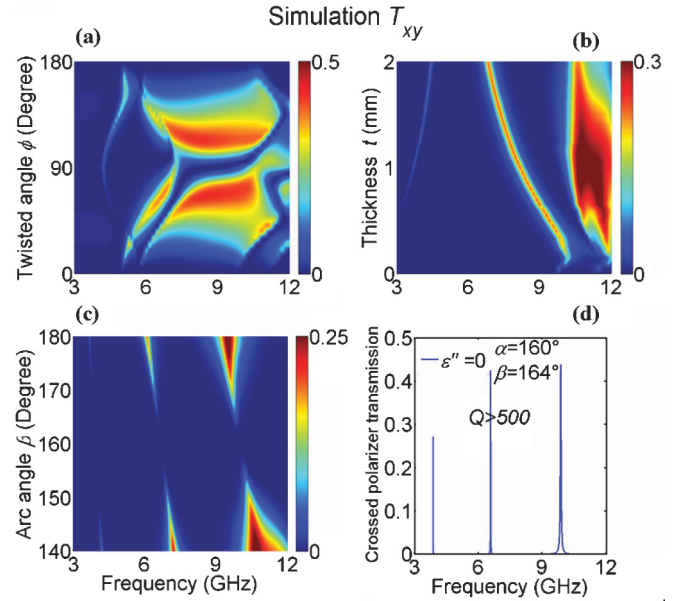

FIG. 4. (Color online) Engineering stereometamaterial-based polarization spectral filters. Simulated transmission spectra as a function of (a) twist angle, (b) dielectric-layer thickness, and (c) asymmetry. (d) The transmission of an ultranarrow filter with no loss for $\alpha = 160°$ and $\beta = 164°$.

The resonant frequencies of the three passbands redshifts with the increasing arc angle β, and the reducing asymmetry as β approaches $160°$ results in decreases of both bandwidth and transmission peak amplitude. The transmission amplitude is mainly limited by dielectric losses. An appropriate choice of low-loss PCB material is helpful to suppress such losses. When we assume that the imaginary part of the dielectric constant tends to zero, the small asymmetry of $\alpha = 160°$ and $\beta = 164°$ allows triple-band ultranarrow cross-polarization transmission for the stereometamaterial with twist angle of $\phi = 90°$, as shown in Fig. 4(d). The quality factor calculated by $Q = f/\Delta f$ is larger than 500. If a low-loss dielectric material such as Roger 5880 is selected, it is possible to achieve high performance of multiband stereometamaterial-based polarization spectral filters. Since silicon exhibits low loss in the terahertz regime, where metals are approximately perfect conductors, the proposed scheme is also suitable for terahertz polarization spectral filters.

We focus on the response of the stereometamaterial with the twist angle of $\phi = 90°$. In terms of circular transmission coefficients, the resonant features can be further studied. The circular transmission matrix can be calculated from the linear transmission matrix using the following basis transformation[15]

$$
\begin{pmatrix} t_{++} & t_{+-} \\ t_{-+} & t_{--} \end{pmatrix}
$$
$$
= \frac{1}{2} \begin{pmatrix} t_{xx} + t_{yy} + i(t_{xy} - t_{yx}) & t_{xx} - t_{yy} - i(t_{xy} + t_{yx}) \\ t_{xx} - t_{yy} + i(t_{xy} + t_{yx}) & t_{xx} + t_{yy} - i(t_{xy} - t_{yx}) \end{pmatrix}
$$
(1)

where t_{jk} is the linear transmission coefficient, $T_{jk} = |t_{jk}|^2$, "$+$" and "$-$" denote the right-handed circularly polarized wave (RCP) and the left-handed circularly polarized wave (LCP), respectively. The simulated amplitude and phase
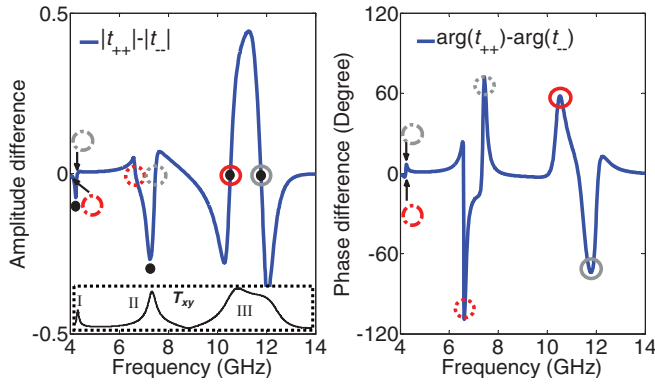
FIG. 5. (Color online) The amplitude and phase differences for circular polarizations transmitted through the stereometamaterial with the twist angle $\phi = 90°$. The solid, dotted, and dash-dotted circle pairs indicate the locations of pure circular birefringence points. Solid dots indicate the positions of crossed polarizer transmission peaks. The inset in the dashed rectangle shows simulated crossed polarizer transmission of the stereometamaterial. I, II, and III denote the three passbands of the stereometamaterial.

differences for RCP and LCP are presented in Fig. 5 to illustrate the 90°-twisted stereometamaterial. Since the proposed stereometamaterial does not show linear birefringence and dichroism, it shows pure optical activity at all frequencies, which manifests itself as circular dichroism (RCP-LCP transmission amplitude difference) and circular birefringence (RCP-LCP phase difference causing polarization rotation). It is interesting that there are multiple pure circular birefringence points marked by solid, dotted, and dash-dotted circle pairs in Fig. 5, where the metamaterial rotates the incident polarization state without changing its ellipticity. The stereometamaterial with twist angle of $\phi = 90°$ has three crossed polarizer transmission bands marked by I, II, and III in the inset of Fig. 5. In fact, the transmission band III centered at a maximum of circular dichroism has two peaks, one weaker than the other. The two peaks of the transmission band III coincide with pure circular birefringence points; however, the single peaks of the transmission bands I and II coincide with the maxima of circular dichroism. In Ref. 20, a single-layer metallic metamaterial only has an isolated transmission band centered at an isoindex point exhibiting pure circular birefringence. For our stereometamaterial, all cross-polarization transmission bands are centered at the maxima of circular dichroism, just lying between a pair of pure circular birefringence points.

Through numerical simulations and experiments, the physical origin of the cross-polarization transmission can be traced to the near-field electric and magnetic coupling between two orthogonal ASRs. High-Q subradiant modes formed by the counterpropagating currents in each ASR layer dominate the low and medium cross-polarization transmission. For 90°-twisted stereometamaterial, circular currents in one ASR with wires perpendicular to incident electric field cannot be directly excited by the incident wave due to its orientation, the so-called "dark element." Nevertheless, for the coupled dimer system, on resonance, the excitation from one ASR can be transferred to the other by the interaction between two ASRs regardless of retardation effects. Interestingly, because the electric fields in the slit gaps of two ASRs are perpendicular
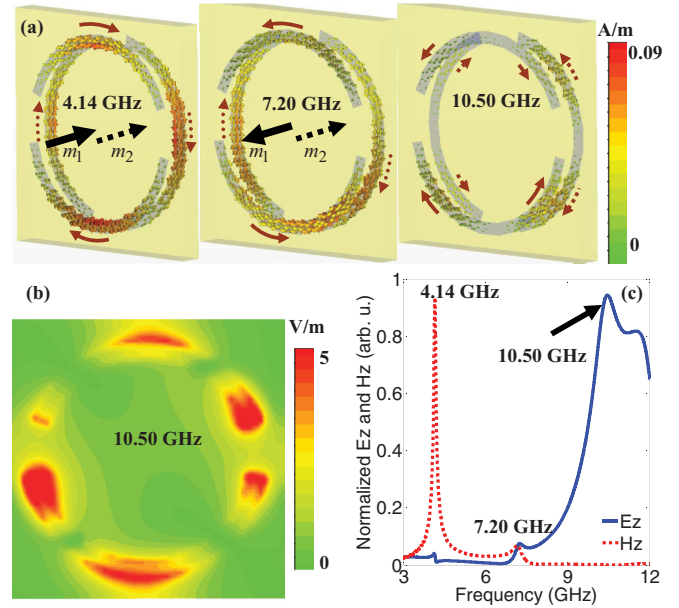

FIG. 6. (Color online) Resonant modes for the cross-polarization transmission peaks of the stereometamaterial with the twist angle $\phi = 90°$. (a) The surface current distribution. The modes correspond to resonance peaks of the crossed transmission marked in Fig. 2(b). Bold arrows qualitatively indicate the direction of excited magnetic dipole m_1 and m_2. Solid and dashed thin arrows indicate the directions of surface currents along ASRs in different layers. (b) The absolute electric-field distribution of cross-polarization transmission peak in the xy plane between two ASRs (middle) at 10.50 GHz. (c) The local electric and magnetic fields as detected by probes lying at the center of a dark element of ASR along the z axis.

to each other, the electric dipole-dipole interaction equals zero. In addition, as the higher-order multipole interaction is negligible, the electric coupling in the twisted ASR dimer can thus be ignored at low frequencies. As a consequence, the resonance levels are determined by the longitudinal magnetic dipole-dipole coupling.

As shown in Fig. 6(a), at the resonances of 4.14 and 7.20 GHz, the resulting magnetic dipoles in the ASR dimer are aligned parallel and antiparallel, respectively, due to the hybridization of magnetic resonances.[27] When the frequency approaches the resonant peak at 10.50 GHz, the circular currents vanish in each ASR, and therefore no magnetic dipole resonance is induced. However, there is strong higher-order electric multipole coupling between 90°-twisted ASRs that enhances the electric resonance. This is seen from the electric fields, E_z, in the xy plane between two ASRs, as demonstrated in Fig. 6(b). To study the local magnetic and electric fields, we place the probes at the center of ASR with the dark element and vary the incident frequency. As clearly seen in Fig. 6(c), the magnetic field H_z at 4.14 GHz is much stronger than that at 7.20 GHz, and the magnetic field at 10.50 GHz goes to zero; however, the electric field E_z at 10.50 GHz is much stronger than that at any other frequencies, which is in good agreement with the results of near-field coupling.

In summary, we have demonstrated numerically and experimentally that multiband polarization spectral filters can be achieved by twisted ASRs stereometamaterials based on the near-field electric and magnetic coupling effects. The

cross-polarization transmission bands are centered at the maxima of circular dichroism, accompanied by pairs of pure circular birefringence points. In particular, we have realized ripples-free cross-polarization transmission bands that can be engineered via the (i) twist angle and (ii) geometrical asymmetry of the ASRs, as well as the (iii) substrate's thickness and dielectric constant. We have shown that dynamic tuning is possible via the angle of incidence. These structures are compatible with established microfabrication and nanofabrication technologies. Moreover, recent progress in plasmonic metamaterials promises opportunities to modulate and tune properties of such filters. We predict that multiple ultranarrow-band polarization spectral filters can be realized using low-loss dielectric substrate and that this technology can be extended to the terahertz and infrared spectral ranges.

*Corresponding author: hrbeusjh@gmail.com

†tjcui@seu.edu.cn

[1] D. R. Smith, J. B. Pendry, and M. C. K. Wiltshire, Science **305**, 788 (2004).

[2] Y. M. Liu and X. Zhang, Chem. Soc. Rev. **40**, 2494 (2011).

[3] N. I. Zheludev, Science **328**, 582 (2010).

[4] J. Hao, Y. Yuan, L. Ran, T. Jiang, J. A. Kong, C. T. Chan, and L. Zhou, Phys. Rev. Lett. **99**, 063908 (2007).

[5] M. Beruete, M. Navarro-Cia, M. Sorolla, and I. Campillo, J. Appl. Phys. **103**, 053102 (2008).

[6] J. Y. Chin, M. Z. Lu, and T. J. Cui, Appl. Phys. Lett. **93**, 251903 (2008).

[7] J. K. Gansel, M. Thiel, M. S. Rill, M. Decker, K. Bade, V. Saile, G. von Freymann, S. Linden, and M. Wegener, Science **325**, 1513 (2009).

[8] M. Mutlu, A. E. Akosman, A. E. Serebryannikov, and E. Ozbay, Opt. Lett. **36**, 1653 (2011).

[9] J. Y. Chin, J. N. Gollub, J. J. Mock, R. P. Liu, C. Harrison, D. R. Smith, and T. J. Cui, Opt. Express **17**, 7640 (2009).

[10] Y. Q. Ye and S. L. He, Appl. Phys. Lett. **96**, 203501 (2010).

[11] L. V. Alekseyev, E. E. Narimanov, T. Tumkur, H. Li, Yu. A. Barnakov, and M. A. Noginov, Appl. Phys. Lett. **97**, 131107 (2010).

[12] V. A. Fedotov, P. L. Mladyonov, S. L. Prosvirnin, A. V. Rogacheva, Y. Chen, and N. I. Zheludev, Phys. Rev. Lett. **97**, 167401 (2006).

[13] S. Zhang, Y. S. Park, J. Li, X. Lu, W. Zhang, and X. Zhang, Phys. Rev. Lett. **102**, 023901 (2009).

[14] E. Plum, J. Zhou, J. Dong, V. A. Fedotov, T. Koschny, C. M. Soukoulis, and N. I. Zheludev, Phys. Rev. B **79**, 035407 (2009).

[15] J. Zhou, J. Dong, B. Wang, Th. Koschny, M. Kafesaki, and C. M. Soukoulis, Phys. Rev. B **79**, 121104(R) (2009).

[16] A. V. Rogacheva, V. A. Fedotov, A. S. Schwanecke, and N. I. Zheludev, Phys. Rev. Lett. **97**, 177401 (2006).

[17] M. Decker, M. Ruther, C. E. Kriegler, J. Zhou, C. M. Soukoulis, S. Linden, and M. Wegener, Opt. Lett. **34**, 2501 (2009).

[18] Z. Li, K. B. Alici, E. Colak, and E. Ozbay, Appl. Phys. Lett. **98**, 161907 (2011).

[19] C. H. Henry, Phys. Rev. **143**, 627 (1966).

[20] N. I. Zheludev, E. Plum, and V. A. Fedotov, Appl. Phys. Lett. **99**, 171915 (2011).

[21] N. Liu, H. Liu, S. N. Zhu, and H. Giessen, Nat. Photonics **3**, 157 (2009).

[22] E. Plum, V. A. Fedotov, A. S. Schwanecke, N. I. Zheludev, and Y. Chen, Appl. Phys. Lett. **90**, 223113 (2007).

[23] E. Plum, V. A. Fedotov, and N. I. Zheludev, Appl. Phys. Lett. **93**, 191911 (2008).

[24] CST Microwave Studio 2010.

[25] V. A. Fedotov, M. Rose, S. L. Prosvirnin, N. Papasimakis, and N. I. Zheludev, Phys. Rev. Lett. **99**, 147401 (2007).

[26] V. A. Fedotov, A. Tsiatmas, J. H. Shi, R. Buckingham, P. de Groot, Y. Chen, S. Wang, and N. I. Zheludev, Opt. Express **18**, 9015 (2010).

[27] H. Liu, D. A. Genov, D. M. Wu, Y. M. Liu, Z. W. Liu, C. Sun, S. N. Zhu, and X. Zhang, Phys. Rev. B **76**, 073101 (2007).

[28] M. Liu, D. A. Powell, I. V. Shadrivov, and Y. S. Kivshar, Appl. Phys. Lett. **100**, 111114 (2012).